Pergamon

0301-9322(94)00083-2

Int. J. Multiphase Flow Vol. 21, No. 3, pp. 351–363, 1995

0301-9322/95 $9.50 + 0.00

A TRANSIENT TWO-FLUID MODEL FOR THE SIMULATION OF SLUG FLOW IN PIPELINES—II. VALIDATION

V. DE HENAU† and G. D. RAITHBY

Department of Mechanical Engineering, University of Waterloo, Waterloo, Ontario, Canada N2L 3G1

(Received 29 July 1993; in revised form 3 November 1994)

Abstract—This is the second of two papers which discuss a transient two-fluid model for the simulation of slug flow in pipelines. In the first paper, new constitutive relations for the drag coefficient and the virtual mass force for the slug flow regime were derived. To account for the non-uniform distribution of the phases and of the pressure drop along a slug unit, new coefficients in the pressure gradient term in the momentum conservation equations for the gas and the liquid phases were also obtained. In this paper, the new components of the transient two-fluid model are validated by comparing the model predictions for gas (or liquid) fractions and pressure drops for steady-state and transient slug flow in pipes to available numerical and experimental data. These comparisons show the potential of the present approach to predict general transient slug flow problems in pipelines.

Key Words: gas–liquid flow, two-fluid models, slug flow, transient, pipeline, drag coefficient, virtual mass force, constitutive relations

1. INTRODUCTION

In the companion paper (De Henau & Raithby 1995), referred to in the following as part I, a one-dimensional transient two-fluid model is developed to predict slug flow in pipelines. To account for the interphase interactions through momentum transfer, new constitutive relations for the drag coefficient and the virtual mass force for the slug flow regime are derived by applying the conservation equations to a geometrically simplified slug unit. In addition, new coefficients in the pressure gradient term in the two-fluid momentum equations are also obtained to account for the non-uniform distribution of the phases and of the pressure drop along a slug unit. Because the new relations are based on the basic conservation principles, this model is believed to more accurately treat the hydrodynamics of slug flow than traditional two-fluid models (e.g. Richards *et al.* 1985).

In this paper, the new components of the two-fluid model are validated by comparing the present two-fluid model predictions for gas or liquid fractions and pressure gradients to available numerical and experimental data under the following conditions:

(1) steady-state air–water slug flow in a horizontal pipe
(2) steady-state air–oil slug flow in horizontal and inclined pipes
(3) transient air–water slug flow in a horizontal pipe.

In section 2 of this paper the numerical model used to solve the differential transport equations is described. This is followed by the validation study itself, which concludes that the model predictions are in generally good agreement with data for various test problems.

2. THE NUMERICAL MODEL

In order to solve the differential transport equations ([1] and [2] in part I) for the gas and the liquid phases, a numerical method is required. In a first step, the pipeline is subdivided into finite volumes, as illustrated in figure 1. The control volumes can be of different lengths, denoted

†Present address: GEC ALSTHOM Electromécanique, 1500 rue Vandral, Tracy, Québec, Canada J3R 5K9.

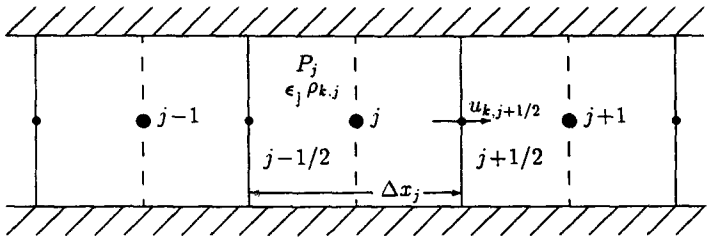

Figure 1. Typical finite difference grid for a pipeline section.

by Δx_j. In this work, the staggered grid arrangement of Patankar (1980) is chosen where the scalar variables and the pressure are stored at the center of the "scalar" or "continuity control volumes"; the boundaries of these volumes are denoted by the full lines in figure 1, and identified by the node index j. The phase velocities are stored at the faces of the scalar control volumes, in the "momentum control volumes", with faces denoted by the dashed lines in figure 1, and identified by node indices like $j + 1/2$. The staggered grid arrangement eliminates the decoupling in the pressure field that can occur when the pressure and the velocity are stored at coinciding nodes.

The second step of the numerical method consists of integrating the differential transport equations over the length of the control volumes and over time to yield a set of linear algebraic equations. A time implicit scheme is chosen to relax the severe time step restriction that results from time explicit schemes. The convected variables are related to the nodal values by a full upwind difference scheme (UDS). Because of the large number of non-linearities found in the equations of the two-fluid model, it can be very difficult to identify the source of numerical instabilities in the flow solutions. Although UDS is a first order scheme in space, and may often be less accurate than higher order schemes, it eliminates the sources of instabilities associated with those higher order schemes. The inaccuracy in the solution that results from UDS can be removed by using finer meshes.

Newton linearization is applied to the integral equations and, after introducing the discrete approximations, the algebraic equations for mass and momentum become:

mass conservation for phase k in control volume j

$$a^{c,k}_{1,j}\epsilon_j + a^{c,k}_{2,j}\epsilon_{j+1} + a^{c,k}_{3,j-1}\epsilon_{j-1} + a^{c,k}_{4,j}u_{k,j+1/2} + a^{c,k}_{5,j}u_{k,j-1/2} + a^{c,k}_{6,j}\rho_{k,j} + a^{c,k}_{7,j}\rho_{k,j+1} + a^{c,k}_{8,j}\rho_{k,j-1} = b^{c,k}_j \quad [1]$$

momentum conservation for phase k in control volume $j + 1/2$

$$a^{m,k}_{1,j+1/2}\epsilon_j + a^{m,k}_{2,j+1/2}\epsilon_{j+1} + a^{m,k}_{3,j+1/2}\epsilon_{j-1} + a^{m,k}_{4,j+1/2}u_{G,j+1/2} + a^{m,k}_{5,j+1/2}u_{G,j+3/2} + a^{m,k}_{6,j+1/2}u_{G,j-1/2}$$
$$+ a^{m,k}_{7,j+1/2}u_{L,j+1/2} + a^{m,k}_{8,j+1/2}u_{L,j+3/2} + a^{m,k}_{9,j+1/2}u_{L,j-1/2} + a^{m,k}_{10,j+1/2}P_j + a^{m,k}_{11,j+1/2}P_{j+1} = b^{m,k}_{j+1/2} \quad [2]$$

In [1], $a^{c,k}_{1,j}$, $a^{c,k}_{2,j}$, ..., $a^{c,k}_{8,j}$, $b^{c,k}_j$ are the coefficients for the linear continuity equation for phase k ($k = G$ for the gas phase, $k = L$ for the liquid phase) for the control volume j. The coefficients $a^{m,k}_{1,j+1/2}$, $a^{m,k}_{2,j+1/2}$, ..., $a^{m,k}_{11,j+1/2}$, $b^{m,k}_{j+1/2}$ in [2] are for the linear momentum equation for phase k in the control volume $j + 1/2$. ϵ is the gas void fraction, u_k is the axial velocity of phase k and P is the average pressure over the cross-sectional area A of the pipeline.

The equation of state is also required and is written for node j as:

$$\rho_{G,j} = \frac{P_j}{\mathscr{R}T} \quad [3]$$

where $\mathscr{R}$ is the gas constant and T is the temperature.

To complete the numerical model, boundary conditions are needed at the inlet and outlet of the pipeline. In general, for pipeline two-phase flow calculations, the inlet mass flow rates for the gas and the liquid phases are specified while, at the outlet, zero gradients for the phase velocities and the gas fraction are used. The pressure is also specified at the pipeline outlet.

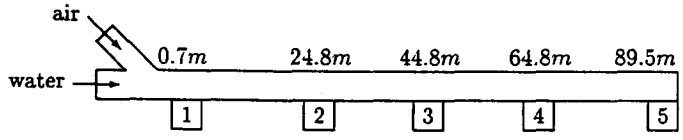

Figure 2. Schematic of the test section for steady-state air–water slug flow in a horizontal pipe.

For a given time t, the linear equation set is solved with a direct block tridiagonal solver. Because a direct solver is used, the coupling between the equations remains active, which is needed to obtain a good convergence behaviour. Once the solution for time t is obtained, a convergence test is performed to check if a steady-state solution has been reached. If it has not, and if the present maximum time level has not been achieved, the time is increased by Δt, the coefficients in [1] and [2] are updated and the procedure is repeated.

A full description of the derivation of the coefficients of [1] and [2] and of the solution procedure is found in the work of De Henau (1992).

In the following section, the results from the validation study are presented.

3. THE MODEL VALIDATION

3.1. Steady-state air–water slug flow in a horizontal pipe

3.1.1. Description of the problem. In this validation problem, the two-fluid model predictions for gas fraction and pressure drop are compared to the experimental data of Théron (1989) for steady-state air–water slug flow in a horizontal pipe. A simplified schematic of the test section is given in figure 2. The PVC pipe has an inside diameter of 53 mm and a length of 89.9 m. Air and water are introduced separately, as shown in the figure. The measurement stations 1 to 5 are also shown in figure 2.

The air is treated as a compressible isothermal gas. The following fluid properties are used in the numerical simulation: water density $\rho_L = 998.2$ kg/m^3, water viscosity $\eta_L = 9.930 \times 10^{-4}$ Ns/m^2, air viscosity $\eta_G = 1.824 \times 10^{-5}$ Ns/m^2, surface tension $\sigma = 0.073$ N/m. The experimental values for temperature and atmospheric pressure are given by Théron (1989).

3.1.2. Implementation of the numerical model. Because the spatial gradients along the pipe are not very large, the number of control volumes used in the numerical model for this test case has a negligible influence on the predictions. For the results presented here, the pipe is divided into 90 control volumes.

The air and the water mass flow rates are specified from the measured inlet superficial velocities and the inlet gas fraction is evaluated by extrapolation from downstream values.

The outlet experimental pressure, P_{out}, is not given. In the model, P_{out} is therefore set such that the predicted pressure at station 3 matches the experimental value given by Théron (1989). P_{out} is always within $\pm 3\%$ of 0.1 MPa.

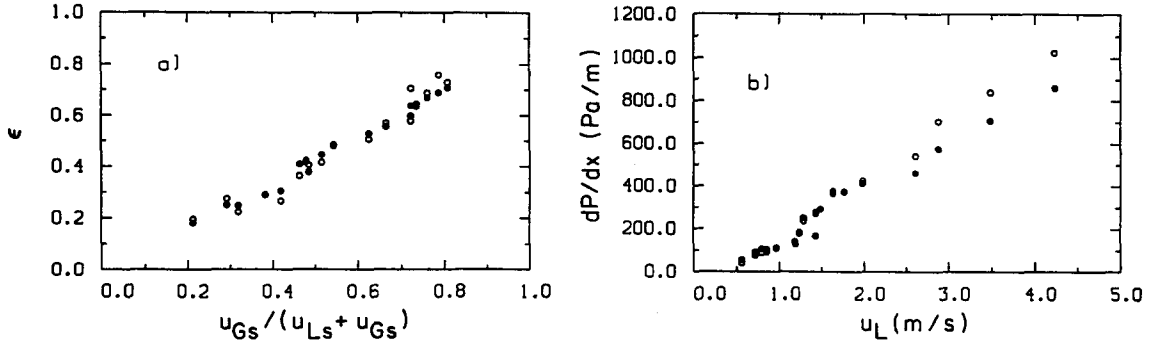

Figure 3. (a) Average gas fraction for steady-state air–water slug flow in a horizontal pipe; (b) average pressure gradient for steady-state air–water slug flow in a horizontal pipe. ○, Experimental data (Théron 1989); ●, predictions of the present model.

The predicted gas fractions used for the comparisons with the data are the average of the gas fractions from stations 1 to 5. The predicted pressure gradients reported here are the average of the pressure gradient between stations 1 and 3 and between stations 3 and 5. The predictions used are from the steady-state solutions to the model.

3.1.3. Presentation and discussion of the results. The comparisons between the predicted and the experimental gas fractions, ϵ and pressure gradients, dP/dx are illustrated in figure 3. The superficial velocities of the gas and liquid, u_{Gs} and u_{Ls}, and the liquid velocity, u_L, used in figure 3 are the experimental values taken at station 3.

The numerical results agree well with the experimental data. The calculated gas fractions are within $\pm 10\%$ of the measured values. The computed pressure gradients fall within approximately $\pm 15\%$ of the data, with the worst comparisons for the higher liquid velocities.

Théron (1989) noted that the four data points for $u_L > 2.5$ m/s [figure 3(b)] are located in the transition region between the slug and the annular flow regimes. In the present study, the numerical results for those points are obtained for the slug flow regime only. This would therefore explain the discrepancies between the pressure gradient data and the predictions for $u_L > 2.5$ m/s.

3.2. Steady-state air–oil slug flow in horizontal and inclined pipes

3.2.1. Description of the problem. Experiments were conducted by Kokal (1987) for air–oil two-phase flow in 25 m long acrylic pipes. In this section, the two-fluid model predictions for liquid fractions and pressure gradients for steady-state slug flow are compared to the data, and to the predictions, of Kokal (1987) (or Kokal & Stanislav 1989) for pipe diameters of 51.2 and 76.3 mm at inclination angles of 0° and +5°. Details of the experimental apparatus are found in the work of Kokal (1987).

The PVC pipe has an inside diameter of 53 mm. The air is treated as a compressible gas. Kokal (1987) listed the oil properties as:

$$\rho_L = 872.9 - 0.6487T \ (\text{kg/m}^3)$$

$$\eta_L = (12.90 - 0.328T + 0.002623T^2) \times 10^{-3} \ (\text{Ns/m}^2)$$

$$\sigma = 0.0309 \ (\text{N/m}).$$

In the experiments, the temperature T varied between 15 and 30°C. The temperature for each experiment was not given. For the purpose of the present comparisons, an average temperature of 22.5°C is used to calculate the properties of the oil as well as that of the air. The gas density required for the inlet mass flow rate of the air is evaluated at 22.5°C and at an average operating pressure in the pipe of 260 ± 3 kPa.

3.2.2. Implementation of the numerical model. All the predictions are obtained with a solution domain divided into 25 control volumes. As with the previous test problem, the gradients along the pipe are small enough that the number of control volumes has a negligible effect on the accuracy of the results.

The inlet mass flow rates are specified with the inlet gas fraction again evaluated by extrapolation using computed downstream values. At the outlet, the pressure P_{out} is adjusted such that the predicted average pressure in the pipe is equal to the experimental value of 260 ± 3 kPa.

The liquid fractions and pressure gradients used in the comparisons with the experimental data are for fully converged steady-state solutions and represent averages over the pipe length.

3.2.3. Presentation and discussion of the results. The predicted liquid fractions and pressure gradients are compared to the experimental data and to the predictions of Kokal (1987) for the 51.2 mm pipe with inclination angles of 0° and +5° in figures 4 and 5, respectively, and for the 76.3 mm pipe and inclination angles of 0° and +5° in figures 6 and 7, respectively.

Liquid fraction: in general, the present two-fluid model has a tendency to underestimate the average liquid fraction when compared to the experimental data, particularly in the 76.3 mm pipe where differences of up to −25% between the predictions and the measurements are recorded. The model of Kokal gives overall better predictions for the liquid fraction.

Taitel & Barnea (1990a) show that the average liquid fraction in a fully developed steady-state slug flow is a function only of the gas and liquid superficial velocities, u_{Gs} and u_{Ls}, the liquid fraction

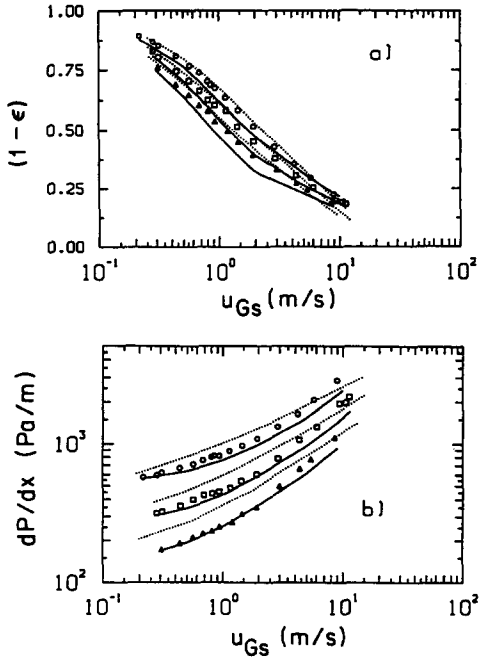

Figure 4. Comparison between experimental data and predictions for steady-state air–oil slug flow with $D = 51.2$ mm and $\theta = 0°$. (a) Average liquid fraction; (b) average pressure gradient. Experimental data (Kokal 1987): △, $u_{Ls} = 0.610$ m/s; □, $u_{Ls} = 0.914$ m/s; ○, $u_{Ls} = 1.372$ m/s; . . , predictions of Kokal (1987); ——, predictions of the present model.

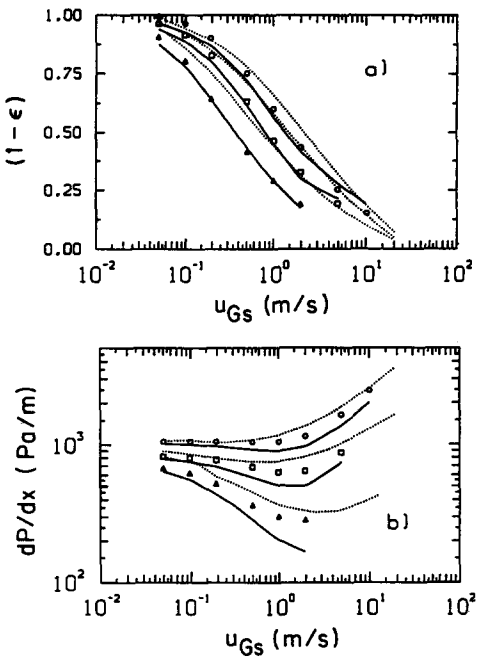

Figure 5. Comparison between experimental data and predictions for steady-state air–oil slug flow with $D = 51.2$ mm and $\theta = +5°$. (a) Average liquid fraction; (b) average pressure gradient. Experiment data (Kokal 1987): △, $u_{Ls} = 0.1$ m/s; □, $u_{Ls} = 0.5$ m/s; ○, $u_{Ls} = 1.0$ m/s; . . , predictions of Kokal (1987); ——, predictions of the present model.

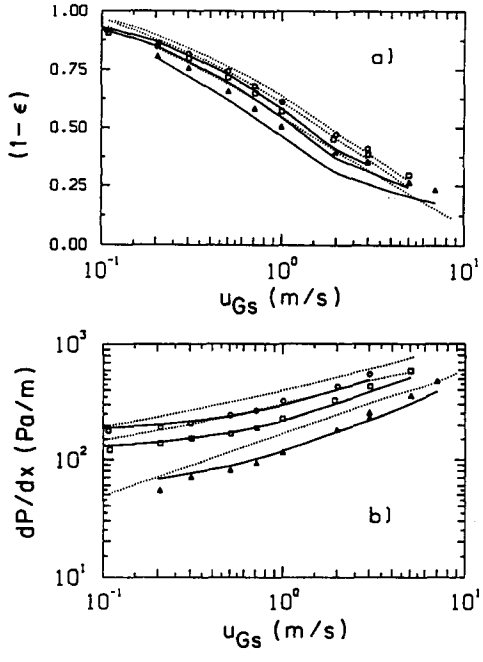

Figure 6. Comparison between experimental data and predictions for steady-state air–oil slug flow with $D = 76.3$ mm and $\theta = 0°$. (a) Average liquid fraction; (b) average pressure gradient. Experimental data (Kokal 1987): △, $u_{Ls} = 0.5$ m/s; □, $u_{Ls} = 0.8$ m/s; ○, $u_{Ls} = 1.0$ m/s; . . , predictions of Kokal (1987); ——, predictions of the present model.

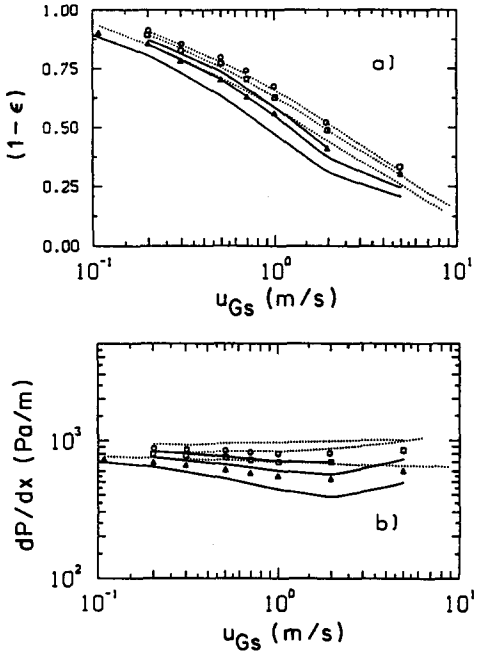

Figure 7. Comparison between experimental data and predictions for steady-state air–oil slug flow with $D = 76.3$ mm and $\theta = +5°$. (a) Average liquid fraction; (b) average pressure gradient. Experimental data (Kokal 1987): △, $u_{Ls} = 0.5$ m/s; □, $u_{Ls} = 0.8$ m/s; ○, $u_{Ls} = 1.0$ m/s; . . , predictions of Kokal (1987); ——, predictions of the present model.

in the slug zone, R_s, and the translational velocity v_t, and is independent of the shape of the film, the film thickness, the film length and the slug zone length. The spatial gradients observed along the pipe for the present test cases are small enough that the flow can be taken as being nearly fully developed. The discrepancies between the present model predictions and the data and predictions of Kokal are therefore likely to be related to the correlations used to calculate R_s and v_t. The correlations utilized by Kokal (1987) (see also Kokal & Stanislav 1989) are different from those employed in the present study. The influence of R_s and v_t on the predictions is discussed later.

Pressure gradient: the present predictions for the pressure gradient compare very well with the data for the horizontal cases [figures 4(b) and 6(b)] falling just slightly below the data for the higher gas velocities. The model of Kokal does not compare as well with the data for these cases.

For the inclined problems [figures 5(b) and 7(b)], the predicted pressure gradients are lower than the experimental values for all the gas and liquid flow rates. Differences of up to -40% between the calculated and the measured values are noted, which is quite significant. For these cases, Kokal's model yields better predictions in terms of the magnitude of the pressure drops. However, the pressure gradient minimum observed in the experimental data as the gas superficial velocity is increased is better reproduced by the present model.

It is believed that the uniform liquid layer approximation for the film zone is again not the main cause for the discrepancies between the present model predictions and the experimental data for the pressure gradient. This approximation affects the film thickness and length as well as the pressure drop in the film zone. A study by Taitel & Barnea (1990b) indicates that the pressure gradients for steady-state slug flow problems obtained with the uniform layer assumption can be higher or lower than predictions obtained with the shape of the liquid film accounted for, but the differences are not significant.

The assumption of a uniform mixture in the liquid slug zone may affect the evaluation of the frictional pressure drop, particularly for the higher flow rates. As the gas flow increases, the amount of gas in the liquid slug zone also increases. In the present model, it is assumed that the bubbles are uniformly distributed in the slug zone with the wall contact area of the gas phase being proportional to the amount of gas. In reality, the bubbles have a tendency to accumulate in the upper portion of the pipe, towards the tail of the liquid slug. The wall contact area of the gas phase may therefore be smaller than the one obtained with the uniform distribution. Overestimating the wall contact area of the gas phase in the liquid slug zone results in a lower frictional pressure drop. This may explain some of the discrepancies that are observed between the present model pressure gradient predictions and the data.

Regarding the influence of the slug length l_s on the pressure gradient predictions, Kokal & Stanislav (1989) found a negligible effect on their results for $20D < l_s < 40D$. Numerical experiments with the present model led to similar conclusions.

It is noticed that the largest discrepancies between the predictions and the data are for the inclined slug flow problems. For these cases, the pressure drop is a function of the frictional losses and the hydrostatic effects. If the liquid fraction is underestimated by the model, the calculated pressure gradient will also be underestimated, as illustrated for example in figure 7. If this is the case, the low predicted pressure gradients must also be related to the inaccuracies in the correlations for R_s and v_t.

The arguments just presented therefore point to inaccuracies in the R_s and v_t correlations as likely reasons for discrepancies between predictions and measurements. The following sections report a study of these factors.

Influence of the R_s correlation: for the purpose of investigating the influence of R_s on the numerical predictions, the results just reported, calculated with the correlation of Andreussi & Bendiksen (1989) ([17] in part I), are compared to new predictions that used the correlation of Gregory *et al.* (1978) given by:

$$R_s = \frac{1}{1 + (v_s/8.66)^{1.39}} \qquad [4]$$

Equation [17] of part I and [4] given above, yield different values of R_s over the range of mixture velocities v_s under consideration. The effect of those differences in R_s on the predictions for the

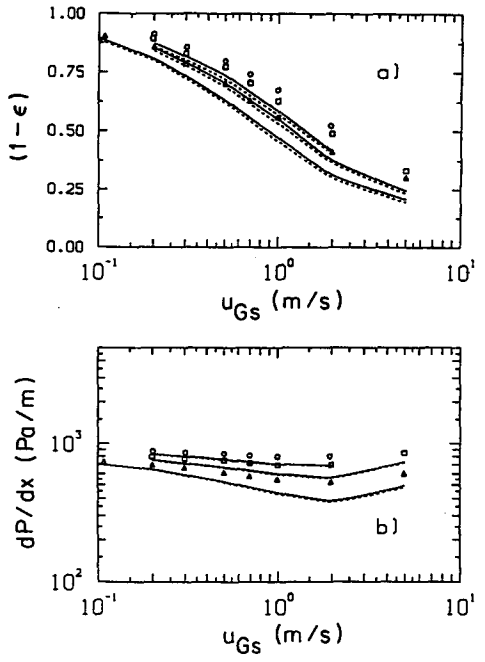

Figure 8. Influence of the R_s correlation on the predictions for air–oil slug flow with $D = 76.3$ mm and $\theta = +5°$. (a) Average liquid fraction; (b) average pressure gradient. Experimental data (Kokal 1987): △, $u_{Ls} = 0.5$ m/s; □, $u_{Ls} = 0.8$ m/s; ○, $u_{Ls} = 1.0$ m/s. Predictions: – – –, with R_s from Gregory *et al.* (1978); ——, with R_s from Andreussi & Bendiksen (1989).

liquid fraction and the pressure gradient are minimal, as illustrated in figure 8 for the 76.3 mm pipe at $+5°$. Similar results were found for the 51.2 mm pipe at $+5°$. Hence, the selection of the R_s correlation does not explain the discrepancies between the present predictions and the data.

Influence of the v_t correlation: the translational velocity of a slug unit is usually evaluated by [14] in part I with several alternative models for the coefficient C_0 and the drift velocity v_d. Kokal (1987) used $C_0 = 1.2$ and evaluated v_d with:

$$v_d = 0.345\left[gD\frac{\rho_L - \rho_G}{\rho_L}\right]^{1/2} \quad [5]$$

which is valid only for vertical slug flow (see Hasan & Kabir 1988).

To investigate the influence of v_t on the numerical results, the present predictions obtained using the correlations of Théron for C_0 and v_d, are compared to the results obtained with v_t evaluated with $C_0 = 1.2$ and v_d estimated by (Bendiksen 1984):

$$v_d = \sqrt{gD}[0.35 \sin\theta + 0.54 \cos\theta] \quad [6]$$

These relations for v_t were also used by Taitel & Barnea (1990b).

There is a strong influence of v_t on the numerical predictions for the liquid fraction, as illustrated in figures 9(a) and 10(a) for $D = 51.2$ and 76.3 mm and $\theta = +5°$. For the smaller pipe diameter [figure 9(a)], the v_t model used by Taitel & Barnea yields liquid fractions that are higher than the experimental data, particularly for the lower liquid flow rate. This results in an important increase in the pressure gradient, as illustrated in figure 9(b). The pressure gradient predictions compare better with the data but this is a consequence of the overestimate of the liquid fraction. In the larger pipe however, both the liquid fraction and the pressure gradient predictions obtained with v_t evaluated as Taitel & Barnea agree well with the data (figure 10).

The translational velocity v_t is used to calculate $u_{r(ss)}$ in [23] of part I and therefore affects the magnitude of the drag coefficient for the slug flow regime. This has a direct impact on the evaluation of the gas and liquid fractions in the pipe.

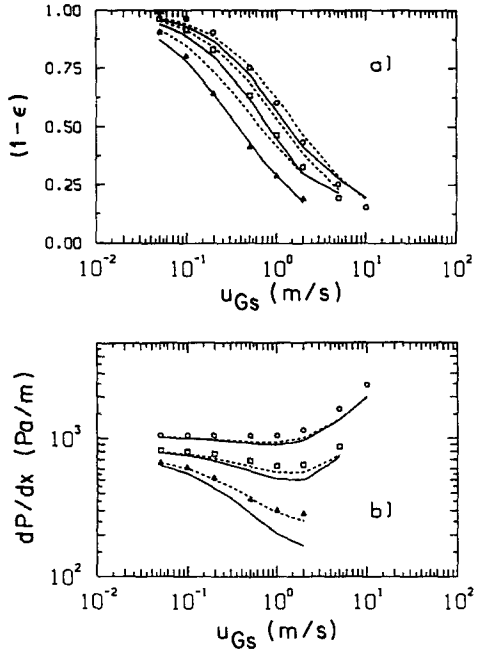

Figure 9. Influence of the v_t correlation on the predictions for air–oil slug flow with $D = 51.2$ mm and $\theta = +5°$. (a) Average liquid fraction; (b) average pressure gradient. Experimental data (Kokal 1987): △, $u_{Ls} = 0.1$ m/s; □, $u_{Ls} = 0.5$ m/s; ○, $u_{Ls} = 1.0$ m/s. Predictions: – – –, with v_t from Taitel & Barnea (1990b); ——, with v_t from Théron (1989).

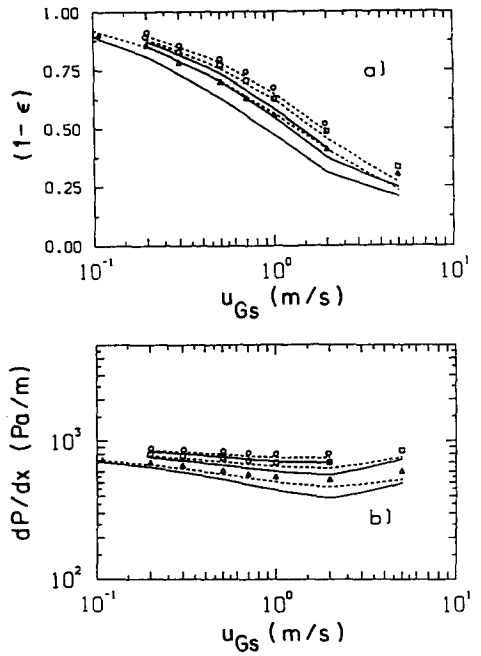

Figure 10. Influence of the v_t correlation on the predictions for air–oil slug flow with $D = 76.3$ mm and $\theta = +5°$. (a) Average liquid fraction; (b) average pressure gradient. Experimental data (Kokal 1987): △, $u_{Ls} = 0.5$ m/s; □, $u_{Ls} = 0.8$ m/s; ○, $u_{Ls} = 1.0$ m/s. Predictions: – – –, with v_t from Taitel & Barnea (1990b); ——, with v_t from Théron (1989).

The correlation of Théron for v_t is based on experimental data for horizontal air–water slug flow and may therefore not be as accurate for inclined slug flow. On the other hand, the correlation recommended by Taitel & Barnea is based on measurements of the velocity of single long bubbles in inclined pipes. The presence of other long bubbles, like in slug flow, may have an influence on the translational velocity. Clearly more research is needed to remove uncertainties related to the prediction of v_t. In the remainder of this paper, the correlations described in part I are used.

3.3. *Transient air–water slug flow in a horizontal pipe*

3.3.1. Description of the problem. Théron (1989) performed several transient air–water slug flow experiments in a horizontal pipe in which he measured the time evolution of the gas fraction, the pressure level and the liquid mass flow rate at the outlet of the pipe, following sudden increases or decreases in the inlet mass flow rates of the gas or the liquid phases. The experiments were carried on in the same PVC pipe which is illustrated in figure 2.

3.3.2. Implementation of the numerical model. The fluid properties used for the numerical simulation are given in section 3.1.1. Steady-state solutions are first obtained for the temperature and superficial velocities u_{Gs} and u_{Ls}, shown in table 1. The outlet pressure is set such that the pressure P_3 in table 1 is satisfied, as described in section 3.1.2. The transient is initiated by suddenly changing the inlet gas or liquid flow rate by the $+\Delta u$ value shown in table 1. After a steady-state is achieved, a second transient is introduced by changing the inlet flow rate by the $-\Delta u$ value in

Table 1. Experimental conditions for transient air–water slug flow in a horizontal pipe

Run No.	u_{Gs} (m/s)	u_{Ls} (m/s)	Δu_{Gs} (m/s)	Δu_{Ls} (m/s)	T (°C)	P_3 (bar)
1	1.120	1.030	±0.360		18.0	0.183
2	0.328	0.506	±0.173		17.5	0.046
3	1.060	0.869		±0.171	18.0	0.147
4	1.110	0.406		±0.206	16.0	0.053

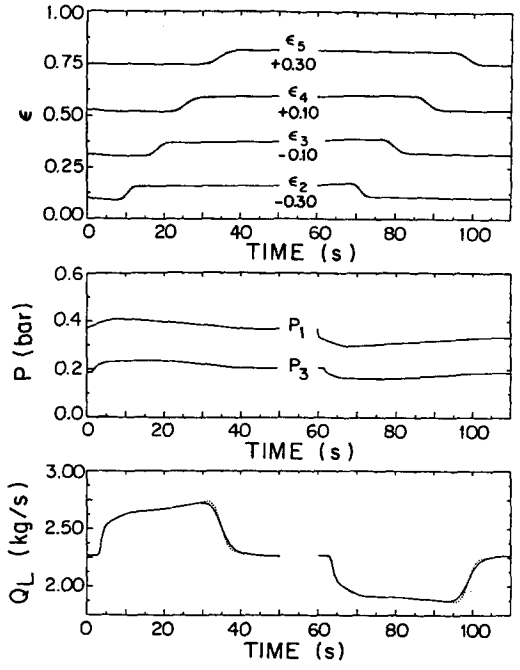

Figure 11. Grid size and time step effects on the time evolution of the gas fraction, pressure and outlet liquid mass flow rate for transient air–water slug flow in a horizontal pipe. Run 1: $u_{Gs} = 1.120$ m/s; $u_{Ls} = 1.030$ m/s; $\Delta u_{Gs} = \pm 0.360$ m/s; $\Delta x_j/\Delta t = 2$ m/s. . . . , $\Delta x_j = 0.1$ m; ——, $\Delta x_j = 0.2$ m.

table 1. The values of ϵ at stations 2 to 5, the pressure at stations 1 and 3 and the outlet liquid flow mass flow rate are recorded during the transients for comparisons with data.

3.3.3. Presentation and discussion of the results.

Sensitivity analysis: to check the grid independence, calculations are performed with different grid sizes and time steps in order to ensure that predictions used for the comparisons with the experimental data are grid size and time step independent. A constant ratio $\Delta x_j/\Delta t = 2$ m/s is chosen, with grid sizes of 0.1, 0.2, 0.4 and 1.0 m. The sensitivity analysis is done for run 1 in table 1.

The numerical results for the time evolution of the gas fraction ϵ, pressure P and outlet liquid mass flow rate Q_L, for the 0.2 and the 0.1 m grids are compared in figure 11. In this figure, the curves for the gas fraction at station 5 (ϵ_5), for example, represent the gas fraction at that station shifted by an indicated value of $+0.30$. Similarly, the curves for ϵ_3 represent the gas fraction at station 3 shifted by a value of -0.10. With this approach, the gas fractions at the different stations can be clearly plotted on the same figure. Note also in figure 11 that the results for the first and second transients are separated by a space on the graphs.

The quantities plotted in figure 11 change little with halving of Δx_j and Δt. The other tests for $\Delta x_j = 0.4$ and 1.0 m give virtually the same pressure distributions, but the sharp variations in ϵ and Q_L with time are somewhat more smeared. Based on these numerical experiments, it is concluded that a grid size of $\Delta x_j = 0.2$ m and a time step of 0.1 s give virtually grid-independent results, except for a slight smearing of the sharp gradients.

Comparisons with experimental data: the comparisons between the present predictions and the experimental data of Théron (1989), for the four runs listed in table 1, are given in figures 12–15. Figures 12 and 13 illustrate cases where transients of different magnitudes are caused by sudden changes in the inlet mass flow rate of the gas phase. Similarly, transients caused by sudden changes in the inlet liquid mass flow rate are shown in figures 14 and 15.

For all the cases, the average gas fraction levels, ϵ, are very well predicted. The wave front velocities are also well predicted although the computed fronts are not as sharp as the experimental data indicate.

The pressure evolution in time is also very well reproduced by the model. The pressure level at station 1 is overpredicted in run 2 (figure 13) but the trends compare favourably with the data.

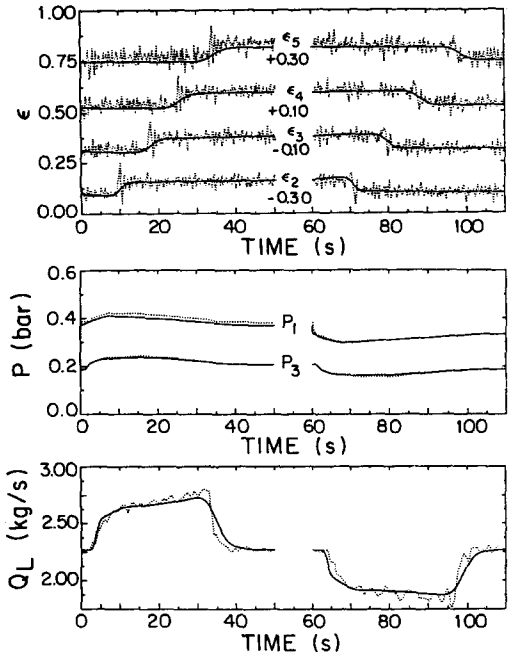

Figure 12. Comparison between experimental data and predictions for time evolution of the gas fraction, pressure and outlet liquid mass flow rate for transient air–water slug flow in a horizontal pipe. Run 1: $u_{Gs} = 1.120$ m/s; $u_{Ls} = 1.030$ m/s; $\Delta u_{Gs} = \pm 0.360$ m/s. . . , experimental data (Théron 1989); ——, predictions of the present model.

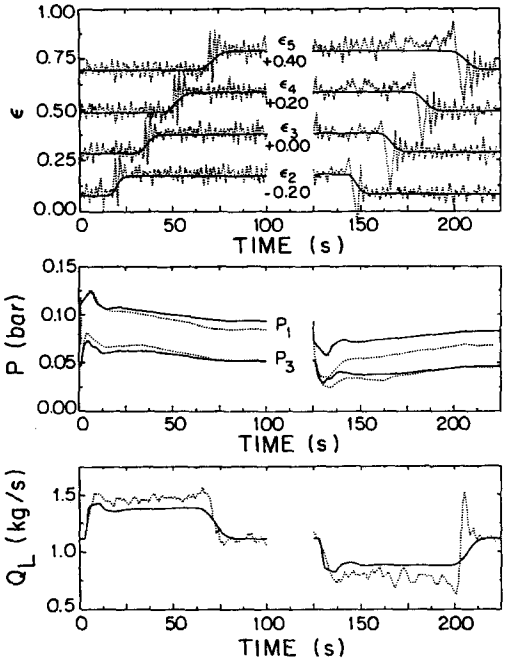

Figure 13. Comparison between experimental data and predictions for time evolution of the gas fraction, pressure and outlet liquid mass flow rate for transient air–water slug flow in a horizontal pipe. Run 2: $u_{Gs} = 0.328$ m/s; $u_{Ls} = 0.506$ m/s; $\Delta u_{Gs} = \pm 0.173$ m/s. . . , experimental data (Théron 1989); ——, predictions of the present model.

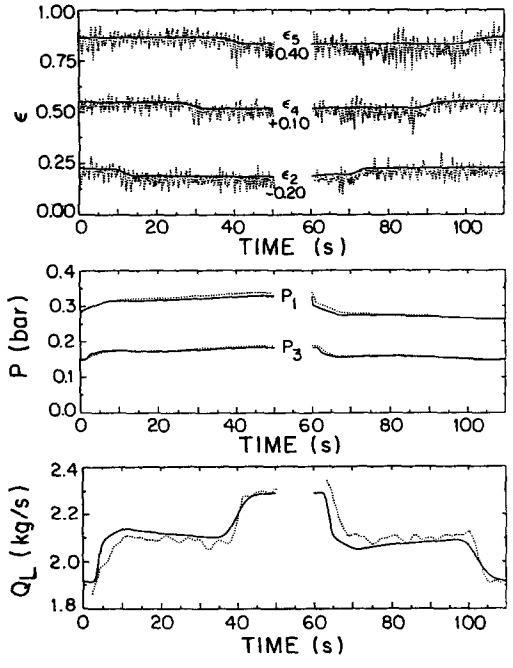

Figure 14. Comparison between experimental data and predictions for time evolution of the gas fraction, pressure and outlet liquid mass flow rate for transient air–water slug flow in a horizontal pipe. Run 3: $u_{Gs} = 1.060$ m/s; $u_{Ls} = 0.869$ m/s; $\Delta u_{Ls} = \pm 0.171$ m/s. . . , experimental data (Théron 1989); ——, predictions of the present model.

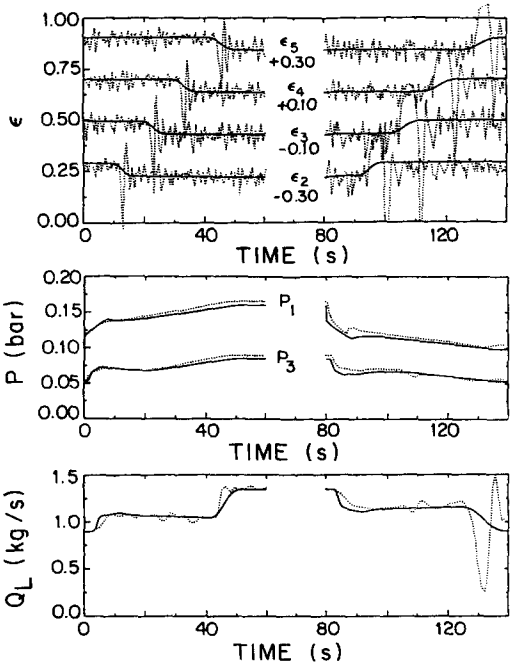

Figure 15. Comparison between experimental data and predictions for time evolution of the gas fraction, pressure and outlet liquid mass flow rate for transient air–water slug flow in a horizontal pipe. Run 4: $u_{Gs} = 1.110$ m/s; $u_{Ls} = 0.406$ m/s; $\Delta u_{Ls} = \pm 0.206$ m/s. . . , experimental data (Théron 1989); ——, predictions of the present model.

It is difficult to isolate the cause of the discrepancies between the predicted and measured pressure levels for this one run. The uniform film approximation, the homogeneous mixture assumption in the slug zone and the correlations for R_s and v_t may be responsible for the discrepancy in the pressure level.

The computed liquid mass flow rates at the outlet of the pipe, Q_L, are also generally in good agreement with the experimental profiles. For most cases, the predicted fronts are not as sharp as the measured ones, which follows from the smearing observed in the calculated gas fraction wave fronts. In some cases, important fluctuations in the liquid mass flow rates, towards the end of the transient periods, are measured (see for example run 4 in figure 15 for $\Delta u_{Ls} = -0.206$ m/s). These fluctuations are caused by variations in the length of the liquid slugs l_s as a result of the transient in the gas or liquid mass flow rates (Théron 1989). Because the present slug flow model assumes a constant slug length of $30D$, such details cannot be predicted.

Comparisons with the predictions of Théron (1989): Théron (1989) developed a mixture model formed of a conservation of mass equation for each phase, a mixture momentum equation and a closure relationship for the average gas velocity which sets $u_G = v_t$.

Figure 16 compares the predictions of Théron (1989) to the present computations for run 1. The results of Théron are obtained with $\Delta x_j = 2.25$ m and $\Delta t = 0.05$ s. The two models give very similar results. Although the same correlations for R_s and v_t have been used in both models, the present computations yield higher gas fractions for the steady-state regions. This is most likely due to the fact that Théron imposes $u_G = v_t$. Equation [22] in part I indicates that, at steady-state, u_G is less than v_t which implies, for a given gas flow rate, a higher gas fraction than for $u_G = v_t$. The higher gas fraction also results in a lower pressure drop due to a reduction in the frictional losses.

From figures 12 and 16, it is seen that the present model predicts more accurately the gas fractions ϵ and the pressure levels than the model of Théron. Similar observations are made from other comparisons between the present model and Théron's model.

Influence of the virtual mass force term: figure 17 compares the predictions of the present model to the results obtained by neglecting the virtual mass force in the momentum equations for run 2.

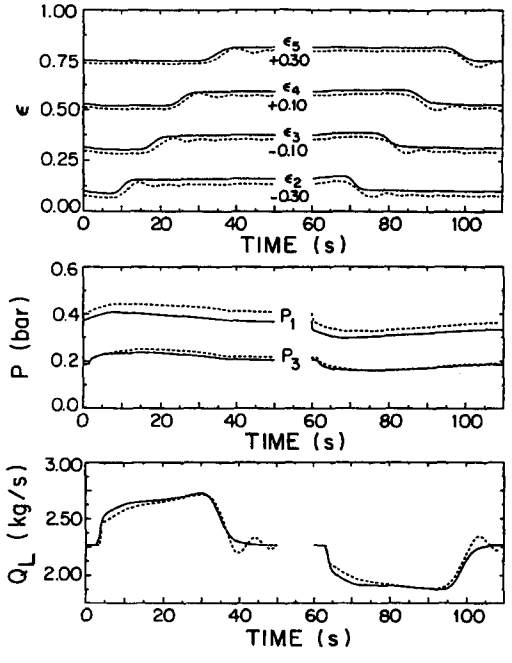

Figure 16. Comparison between predictions of Théron and the present model for time evolution of the gas fraction, pressure and outlet liquid mass flow rate for transient air–water slug flow in a horizontal pipe. Run 1: $u_{Gs} = 1.120$ m/s; $u_{Ls} = 1.030$ m/s; $\Delta u_{Gs} = \pm 0.360$ m/s. – – –, predictions of Théron (1989); ——, predictions of the present model.

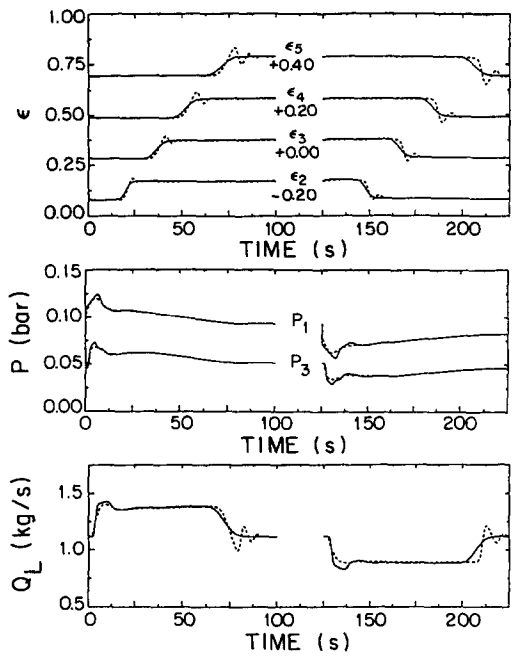

Figure 17. Influence of the virtual mass force on the time evolution of the gas fraction, pressure and outlet liquid mass flow rate for transient air–water slug flow in a horizontal pipe. Run 2: $u_{Gs} = 0.328$ m/s; $u_{Ls} = 0.506$ m/s; $\Delta u_{Gs} = \pm 0.173$ m/s. – – –, predictions with $C_{VM} = 0$; ——, predictions of the present model.

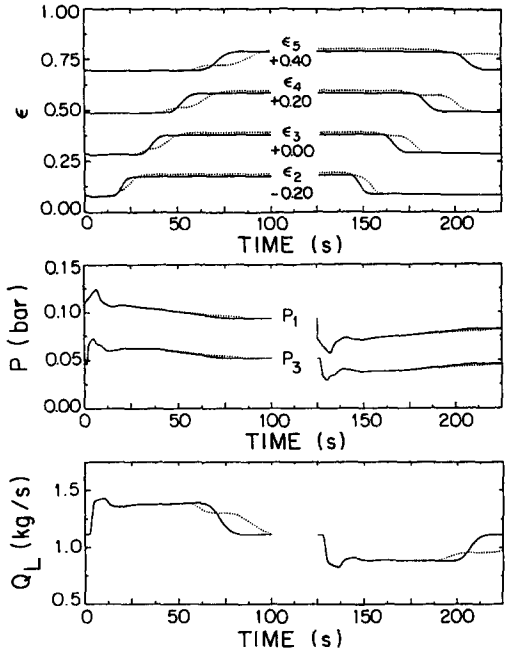

Figure 18. Influence of the virtual mass force on the time evolution of the gas fraction, pressure and outlet liquid mass flow rate for transient air–water slug flow in a horizontal pipe. Run 2: $u_{Gs} = 0.328$ m/s; $u_{Ls} = 0.506$ m/s; $\Delta u_{Gs} = \pm 0.173$ m/s. . . , predictions with the virtual mass force of Ishii & Mishima (1984); ——, predictions of the present model.

The computations are again done with $\Delta x_j = 0.2$ m and $\Delta t = 0.1$ s. It can clearly be seen that neglecting the virtual mass force gives rise to oscillations in the gas fraction waves which appear to grow as the waves propagate downstream. The virtual mass force accounts for the additional inertia felt by the gas phase as it accelerates (or decelerates) the surrounding liquid phase. This additional inertia damps the oscillations, as seen in figure 17.

As a final validation test, figure 18 compares the predictions from the present model to the ones obtained using the virtual mass force proposed by Ishii & Mishima (1984) for run 2 with $\Delta x_j = 0.2$ m and $\Delta t = 0.1$ s. The model of Ishii & Mishima overestimates the virtual mass force, causing the propagation of the gas fraction waves to be delayed compared to the present model (and compared to the experiment also). The strong effect on the shape of the wave fronts influences the time evolution of the liquid mass flow rate at the pipe outlet. Hence, for the transient flow presented here, the virtual mass force approximated by [49] in part I appears to account more accurately for the interaction between the gas and the liquid phases than the model of Ishii & Mishima (1984).

4. CONCLUSIONS

The present paper is concerned with the validation of a one-dimensional transient two-fluid model (De Henau & Raithby 1995) for the prediction of slug flow in pipelines. The new components of the two-fluid model are evaluated by comparing the two-fluid model predictions for steady-state and transient slug flow problems to available numerical and experimental data.

In the case of steady-state air–water slug flow problems in a horizontal pipe, the two-fluid model predictions for gas fractions and for pressure gradients compare well with the experimental data. For air–oil slug flow, important discrepancies are observed between the computed liquid fractions and pressure drops in horizontal and inclined pipes. It is shown, however, that the results are very sensitive to the magnitude of the slug unit translational velocity. It is believed that improving the v_t correlation would improve the accuracy of the two-fluid model for the air–oil slug flow problems.

In the transient air–water slug flow problems in a horizontal pipe, the two-fluid model predictions compare well with the data for the gas fraction, pressure and outlet liquid mass flow rate evolution in time. It is also shown that the virtual mass force can have a significant influence on the numerical predictions for transient slug flow. The virtual mass force model developed in this study accounts properly for the effects of the transients on the interaction between the two phases.

The results from this validation show the potential of the present approach to predict general transient slug flow problems in pipelines.

REFERENCES

ANDREUSSI, P. & BENDIKSEN, K. 1989 An investigation of void fraction in liquid slugs for horizontal and inclined gas–liquid pip flow. *Int. J. Multiphase Flow* **15,** 937–946.

BENDIKSEN, K. 1984 An experimental investigation of the motion of long bubbles in inclined tubes. *Int. J. Multiphase Flow* **10,** 467–483.

DE HENAU, V. 1992 A study of terrain-induced slugging in two-phase flow pipelines. Ph.D. thesis, University of Waterloo, Ontario, Canada.

DE HENAU, V. & RAITHBY, G. D. 1995 A transient two-fluid model for the simulation of slug flow in pipelines—I. Theory. *Int. J. Multiphase Flow* **21,** 335–349.

GREGORY, G. A., NICHOLSON, M. K. & AZIZ, K. 1978 Correlation of the liquid volume fraction in the slug for horizontal gas–liquid slug flow. *Int. J. Multiphase Flow* **4,** 33–39.

HASAN, A. R. & KABIR, C. S. 1988 Predicting multiphase flow behavior in a deviated well. *SPE Prod. Engng* 474–482.

ISHII, M. & MISHIMA, K. 1984 Two-fluid model and hydrodynamic constitutive relations. *Nucl. Engng Des.* **82,** 107–126.

KOKAL, S. L. 1987 An experimental study of two-phase flow in inclined pipes. Ph.D. thesis, University of Calgary, Calgary, Alberta, Canada.

KOKAL, S. L. & STANISLAV, J. F. 1989 An experimental study of two-phase flow in slightly inclined pipes—II. Liquid holdup and pressure drop. *Chem. Engng Sci.* **44,** 681–693.

PATANKAR, S. V. 1980 *Numerical Heat Transfer and Fluid Flow.* Hemisphere, Washington, DC.

RICHARDS, D. J., HANNA, B. N., HOBSON, N. & ARDRON, K. H. 1985 ATHENA: a two-fluid code for CANDU LOCA analysis. *3rd International Conference on Reactor Thermalhydraulics,* Newport, RD, U.S.A.

TAITEL, Y. & BARNEA, D. 1990a Two-phase slug flow. In *Advances in Heat Transfer,* Vol. 20. Academic Press, New York.

TAITEL, Y. & BARNEA, D. 1990b A consistent approach for calculating pressure drop in inclined slug flow. *Chem. Engng Sci.* **45,** 1199–1206.

THÉRON, B. 1989 Ecoulements diphasiques instationnaires en conduite horizontale. Thèse de docteur-ingénieur, Institut National Polytechnique de Toulouse, France.